17th World Conference on Earthquake Engineering, 17WCEE
Sendai, Japan - September 13th to 18th 2020

DYNAMIC CENTRIFUGE TEST OF AN EMBANKMENT UNDERLAIN A LIQUIFIABLE SOIL AND ISOLATED SOIL-CEMENT COLUMNS

M. Khosravi [1], M. Pourakbar [2], A. Soroush [3], S. Zaregarizi [4] ,W. Y. Hung[5], A. Nabizadeh[6]

[1]*Assistant Professor, Department of Civil Engineering, Montana State University USA, mkhosravi@montana.edu*
[2]*Graduate student, Department of Civil and Environmental Engineering, Amirkabir University of Technology IR, mehran.pourakbar@gmail.com*
[3]*Professor, Department of Civil and Environmental Engineering, Amirkabir University of Technology IR, soroush@aut.ac.ir*
[4]*Graduate Student, Department of Civil Engineering, Montana State University USA, shahabzare@yahoo.com*
[5] *Assistant Professor, Department of Civil Engineering, National Central University of Taiwan, wyhung@ncu.edu.tu*
[6] *Assistant Professor, Department of Civil Engineering, Shahid Rajaee Teacher Training University. ali.nabizadeh@ sru.ac.ir*

Abstract

A centrifuge test of an embankment on a loose liquefiable sand layer treated with soil-cement columns was carried out to investigate the effect of soil-cement ground reinforcement on the seismic response of soil and embankment. The test was perfromed at a centrifugal acceleration of 50g with a 3-m radius centrifuge at the National Central University of Taiwan. The model corresponded to, in prototype units, an 8.5-m tall embankment of dense, coarse silica sand with a relative density, D_r, of 80% underlain by a 5.0-m loose saturated silica sand layer with a relative density of 50%. Forty-five isolated soil-cement columns fixed in a concrete base were constructed through the loose sand layer in five rows near the toe of the embankment. The soil-cement had an average unconfined compressive strength of 3.7 MPa, and the columns had an area replacement ratio, A_r, of 27%. The model was shaken with a series of scaled earthquakes having peak base accelerations ranging from 0.03g to 0.55g. This paper briefly describes the model construction procedure (e.g. sand pluviation, soil-cement column construction, instrumentation, etc.) and presents some preliminary results and observations of the performance of soil-cement columns treated embankment.

Keywords: Centrifuge test; Isolated soil-cement column; Seismic response; Embankment; Area replacement ratio

1. Introduction

Mitigation of earthquake damage potential at soft or liquefiable soil sites remains a challenge in earthquake engineering. Soil-cement ground reinforcement techniques have been effectively used to remediate soil embankment and other civil infrastructure against the effects of earthquake-induced liquefaction in their soil foundations. Design issues include the ability of the soil-cement grids to withstand applied forces and stresses without excessive damage in the composite soil and soil-cement system to limit settlements or deformations to acceptable levels. Design methods for soil-cement ground reinforcement, as structural foundations or slope reinforcements, are not as well developed for seismic loading conditions as those for static loading conditions.

Soil-cement columns under an embankment are simultaneously subjected to the vertical compressive load and horizontal load leading to complex modes of failure [1,2]. An isolated soil-cement column may fail by shearing, bending, or tilting depending on the column location and length, soil-cement material strength, embankment height, and loading conditions (e.g. static or seismic). Previous studies have investigated the internal and external failure modes of soil-cement columns and the overlying soil structure under static loading [3,4]. Few studies, however, have documented in detail the effect of soil-cement column reinforcement on seismic response of embankments founded on liquefiable soil reinforced by soil-cement columns [5,6].

Dynamic centrifuge and shaking table tests have been used to investigate the effect of soil-cement ground reinforcement on the stability of soil structures and other ground failure modes in soft or liquefiable soils [7-10]. The results of previous centrifuge tests have indicated that soil-cement columns were relatively

ineffective in stiffening soil profile or reducing the potential for liquefaction triggering. They, however, continued to provide effective support for the structural foundation after liquefaction is triggered [11]. Mengyi et al. [12] used a shaking table test and investigated the performance of discrete soil-cement columns in liquefiable loose sand under a railway embankment. The results of this study showed that the majority of cracking occurred at about 1/3 to 1/2 pile length from the top, and the piles near the toe of the embankment experienced more damage and tilted toward the toe of the embankment. Zhuo et al. [13] studied the performance of the embankments with elastic columns embedded in an inclined underlying stratum using centrifuge testing and numerical modeling. Soil-cement columns with small embedment depth experienced a tilting failure mode while columns with large embedment depth showed limited deflection, and the embankment remained stable after construction. Other studies have suggested that a low strength soil-cement column is expected to fail by shearing, while a high strength soil-cement column is typically expected to fail by tilting and bending instead of shearing [3-4,14-15]. Khosravi et al. [6] and Boulanger et al. [16] investigated the seismic response of an embankment built upon loose liquefiable sand reinforced with soil-cement walls and the potential for cracking and brittle failure in the soil-cement walls. The post-test inspections of the model test illustrated that the loose sand foundation liquefied during strong shaking and the liquefied soil displaced downslope relative to the walls during imposed shaking. Irregular cracking and offsets were observed across the walls that varied along the length of the walls and between the adjacent walls.

This paper summarizes the results of a dynamic centrifuge test examining the seismic response of a soil-cement column supported embankment constructed on a loose layer of liquefiable soil. The test was performed at a centrifugal acceleration of 50 g on the 3-m radius centrifuge at the National Central University of Taiwan. The model corresponded to, in prototype units, an 8.5 m tall embankment of dense, coarse silica sand ($D_r \approx$ 80%) underlain by a 5.0-m thick, saturated loose silica sand layer with D_r of about 50%. Forty-five soil-cement columns in five rows were constructed through the loose sand layer over a 7.8 m long section near the toe and under the embankment. The soil-cement had an average unconfined compressive strength of 3.7 MPa and an area replacement ratio of 27%. The model was subjected to 3 shaking events with base accelerations ranging from 0.03g to 0.55g. The following sections describe the centrifuge model and testing program and a discussion of the soil-cement mixture design and the soil-cement column construction process. Finally, representative recorded responses focusing on the reinforcing effects of the columns, as reflected in the acceleration, pore pressure generation, and settlement responses of the embankment and soil foundation, are presented.

2. Centrifuge test

2.1 Centrifuge Testing Program

A centrifuge test of an embankment model was performed using the 3-m radius centrifuge at the National Central University of Taiwan. The test was performed at a centrifugal acceleration of 50g. The recorded data and model dimensions were converted into prototype units according to the scaling laws, as described by Kutter (1995). All data are presented in prototype units unless otherwise specified.

The test model was performed in a rectangular flexible laminar container. The inner dimensions of the container in the model scale were 71.1 cm long (35.55 m in prototype), 35.6 cm wide (17.8 m in prototype), and 35.5 cm tall (17.75 m in prototype). The container consists of aluminum rings separated by roller bearing in an alternating pattern. The aluminum rings provide lateral confinement for the soil, while the roller bearing maintains continuous shear strain along the direction of loading. Since the container was not watertight, a 3 mm thick rubber membrane (model scale) was attached inside the container to make it watertight.

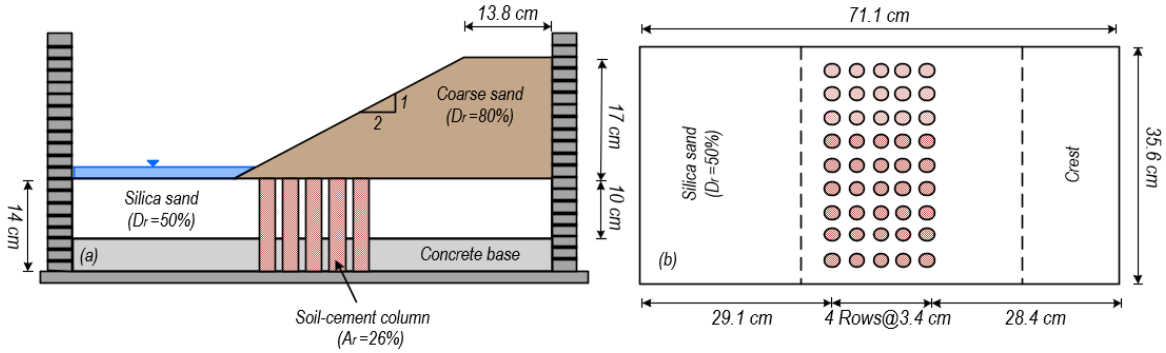

Fig. 1 – 2D model configuration with dimensions in model scale (cm) (a) side view of the embankment model, (b) plan view of the soil foundation

The model consisted of an embankment built upon the loose liquefiable sand reinforced with soil-cement columns, as shown in Fig. 1. Figs. 1a and 1b show a schematic side view and plan view of the model with the dimensions in model scale, respectively. The selected properties of the loose and coarse silica sands are summarized in Table 1. A relatively thick layer (5.0 m) of loose silica sand (D_{50} = 0.193 mm) and a coarse silica sand (D_{50} = 0.32 mm) were used as the material of the liquefiable layer and the embankment, respectively. The model was constructed in multiple layers using dry pluviation at different falling heights (lifts of 2 cm), which were calibrated to the required relative density of the sand layers. The pluviation was interrupted at different locations to place the required sensors (e.g., pore pressure transducer, accelerometers).

Table 1 – Properties of soil used in the model

Soil Type	*Soil Classification*	G_s	$\rho_{max}(\frac{g}{cm^3})$	$\rho_{min}(\frac{g}{cm^3})$	$d_{50}(mm)$	$d_{10}(mm)$
Silica Sand	SP	2.65	1.66	1.41	0.193	0.147
Coarse Sand	SP	2.65	1.63	1.38	0.32	0.3

2.2 Soil-cement Column Construction

A series of forty-five soil-cement columns were constructed from a mixture of soil, cement, and water, with a weight proportion presented in Table 2. After mixing mortar for about 10 min to ensure consistency, the mortar was poured into a mold to form columns having a diameter of 2.0 cm and a height of 14.0 cm. The inside surface of the mold was lubricated to reduce friction between the mold and to facilitate the removal of the columns. The mortar was compacted in five lifts by tapping molding method. Then the columns were placed at a room with a constant temperature of 25 ˚C for about 3 weeks (humidity 90%). In addition to 45 columns, three more specimens were also prepared and cured in the same environment to be used in the unconfined compressive strength (UCS) test. The average UCS of the specimens was 3.7 MPa.

Table 2 – Soil-cement mixtures ratio

Component	Mixture Ratio (by weight)		
	Cement	Sand	Water
Columns	0.28	1	0.24
Base	0.2	1	0.18

A series of five crack detectors (CD) was cast in the soil-cement columns (before curing) at the target locations to monitor the formation and time of cracking in the soil-cement columns during and after shaking, (Fig. 2a). The crack detector is simply a 2-mm pencil lead placed in the longitudinal direction along the column

and connecting to two wires at the ends. Pencil lead has a very small resistance (1-2 Ω) initially that significantly increases when cracking occurrs along the lead. More details can be found in Tamura et al. [18].

After curing, the prefabricated soil-cement columns were removed from the molds and rigidly connected to a cement base with a center-to-center spacing of 34 mm (model scale). The 4 cm cement base layer was constructed by a mortar with a weight proportion of 0.2:1:0.18 for cement, sand, and water, respectively. When the mortar was still soft, the soil-cement columns were placed in a grid pattern with center-to-center spacing of 3.4 cm in predefined locations. A plastic mold was used in the container and above the base to place and hold the soil-cement columns in their position during the installation and curing time of the base layer. A picture of the cement base and soil-cement columns after construction is depicted in Fig. 2a.

Fig. 2 – Soil-cement column construction procedure (a) soil-cement column and crack detectors attached to the cement base (b) soil-cement columns after construction and soil pluviation (c and d) soil foundation before and after saturation

2.3 Model Construction and instrumentation

After placing the pre-fabricated soil-cement columns and curing the cement base, the foundation sand layer and the embankment were constructed in multiple lifts by dry pluviation. The height and opening of the pluviator were calibrated to achieve a D_r of about 50% for the liquefiable sand layer and a D_r of about 80% for the coarse silica sand as the embankment. Fig. 2b illustrates the interrupting of loose silica sand pluviation to place three accelerometers and two pore water pressure transducers in the loose sand layer. A coarse aquarium sand of 1.5 cm thickness (model scale) was then placed in the embankment (about 1.5 cm above the loose sand layer) to prevent the capillary rise of a viscous fluid in the embankment during saturation (Fig. 1c). The saturation process was carried out under vacuum with a viscous fluid have a viscosity approximately 50 times higher than water. The saturation progressed from top of the container to the top of the aquarium sand and took five days. Fig. 2d illustrates the model after saturation. After completion of the saturation of the loose sand layer, the final water level was brought to 1 cm (model scale) above the top of the aquarium sand layer before releasing the vacuum to ensure full saturation of the soil foundation. The container lid was then removed, and the final water level was kept underneath the aquarium sand layer during embankment construction. Pluviation of the embankment was continued, and remaining sensors (e.g., accelerometers and linear potentiometers) were placed at their pre-planned locations. Fig. 3 shows the embankment model after completion.

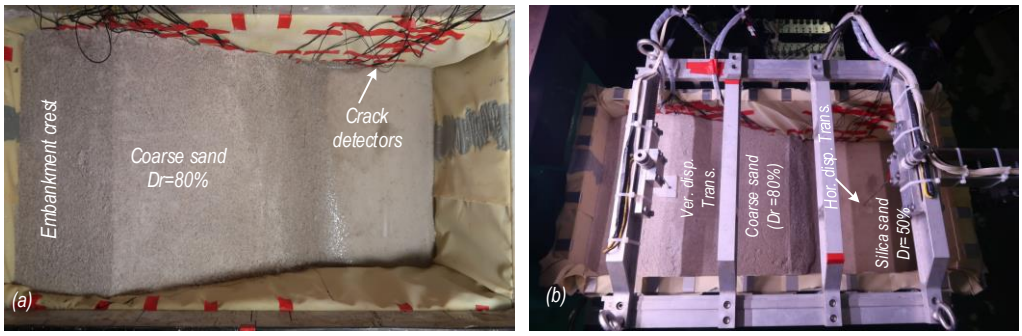

Fig. 3 – Soil-cement column construction procedure (a) Embankment model after construction, (b) configurations of the LP system for vertical displacement measurement of the embankment and the toe

The container then loaded into the centrifuge arm. Two LPs (linear potentiometer) were installed at the crest and downstream of the embankment to monitor the vertical movement. Thin plastic platforms (approximately 40mm × 40mm in plan at model scale) were installed on the sand surface just below the LPs (Fig. 3b). The model was instrumented with three types of transducers used in centrifuge test, including horizontal accelerometers (ACC), pore pressure transducers (PPT), and linear potentiometers (LP). Figs. 4a and 4b show the side and plan views of the locations of select accelerometers, pore pressure transducers, and linear potentiometers. A total of 13 ACCs, 6 PPTs, and 2 LPs were employed in this test.

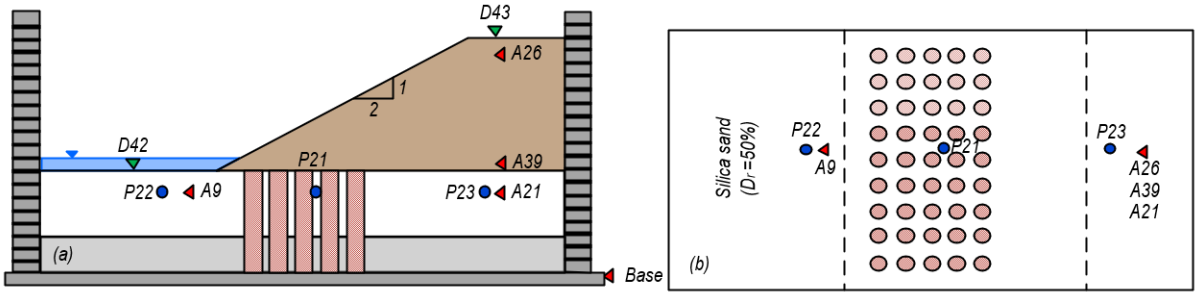

Fig. 4 – 2D model configuration and instrumentation (a) side view of the embankment model, (b) plan view of the soil foundation; accelerometers (red triangle), pore water pressure transducer (blue circle), and displacement transducer (green triangle)

2.4 Input Motions

The model was shaken 3 times with scaled version of 2001 El Salvador earthquake. The first shaking event had a peak base acceleration of PBA=0.03g (in prototype scale), for which the response was elastic and no pore water pressure generated. The second shaking event had a PBA=0.4g, which triggered liquefaction in the saturated sand layer at the toe of the embankment and between the columns, and cracked the soil-cement columns. The third one had a PBA=0.55g which triggered liquefaction in the saturated sand layer and further damaged the columns. Each motion was applied long after dissipation of the pore water pressure from the previous motion.

3. Dynamic Responses

The dynamic responses of the soil-cement ground reinforced system and supported embankment, including the horizontal acceleration responses of the soil foundation and embankment, excess pore water pressure, and soil and embankment deformation, are presented.

3.1 Acceleration Time Histories

The acceleration response of the soil foundation and the embankment are shown in Fig. 5 for El Salvador motion with PBA = 0.4g. Fig. 5a displays the base motion and horizontal motions recorded in the soil near the

toe of the embankment and near the foundation surface (Soil-S9), and in the soil underneath the embankment and near the foundation surface (Soil-S21). Results indicated richer long-period components for the layer of loose sand, which is an indication of liquefaction of the sand layer. The accelerations in the loose sand layer attenuate significantly after the time of approximately 7s during shaking. As shown in Figs. 5b and 5c, the peak horizontal accelerations (PHA) in the soil near the toe of the embankment and near the foundation surface (Soil-S9) and the soil under the embankment and near the foundation surface (Soil-S21) were 0.13 and 0.15g, respectively, which are both smaller than their respective PBA of approximately 0.40g.

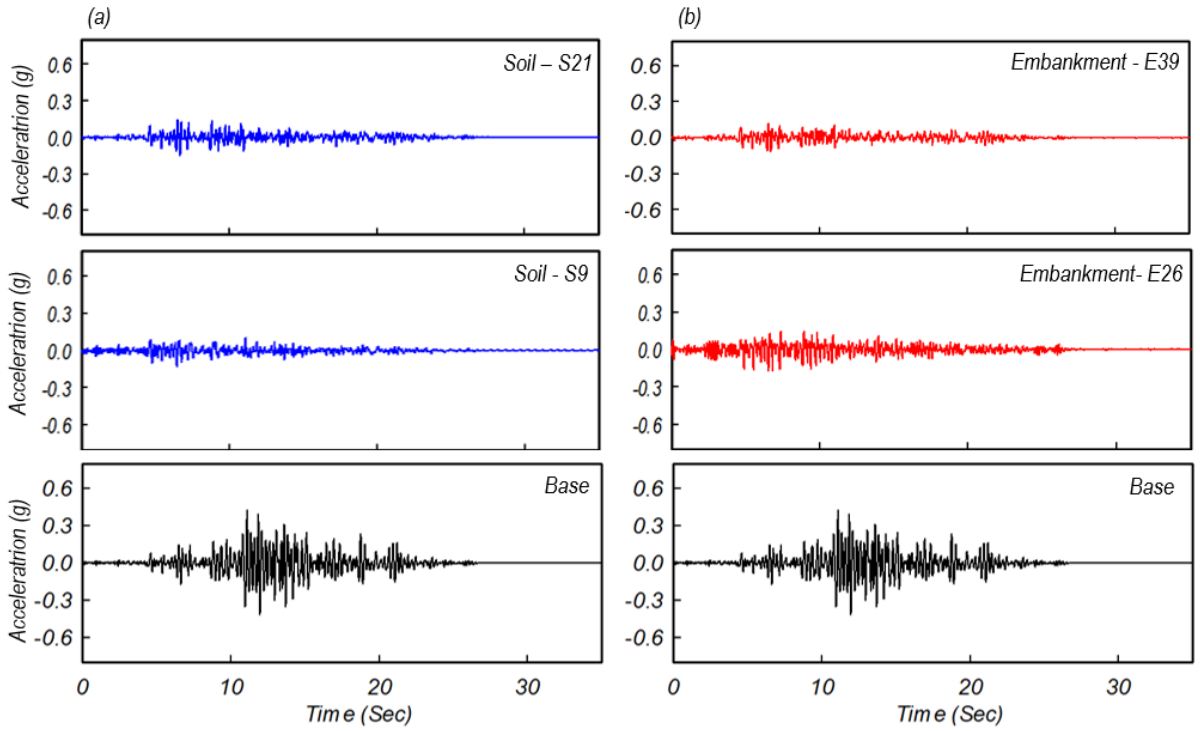

Fig. 5 – Recorded acceleration at the base, embankment and soil foundation during the main shaking with PBA =0.4 g

Fig. 5b shows the base motion and horizontal motions recorded in the embankment and near to the foundation surface (E-39), and on the crest of the embankment (E-26). The recorded peak horizontal acceleration in the embankment and near to the foundation surface was 0.12 g, which was smaller than PBA (≈ 0.4g) due to liquefaction of the soil foundation. The PHAs were amplified up through the embankment reaching a value of 0.17g at the crest during the PBA=0.4g event. The recorded acceleration response at the embankment crest showed a slight asymmetric response due to the occurrence of seismic downslope deformation of the embankment.

3.2 Pore-Water Pressure Time Histories

The excess pore-water pressures (EPWP) measured in the loose sand foundation are shown in Fig. 6 for the same El Salvador motion with PBA = 0.40g. The results include EPWP in the soil underneath the embankment (P23), between the columns (P21), and at the toe of the embankment (P22). As shown in Fig. 6, the EPWP time-history responses could be divided into an initial build-up stage, a sustained level of high excess pore pressures during strong shaking, and a dissipation stage. Unlike the EPWPs measured in the soil at the toe of the embankment (P22) and between the columns (P21), the EPWP in the soil underneath the embankment and near the soil surface (P23) continued to rise beyond the strong shaking period of the motion (time ~20 s) which could be attributed to upward flow of pore water during shaking. The measured excess pore water pressure in the soil underneath the embankment (P23) reached a peak value of 120 kPa, which was far greater than what measured in the free field beyond the toe of the embankment (P22), reflecting the differences in overburden

stresses at these points. The EPWP values in the soil between the columns (P21) and at the toe of the embankment (P22) raised to values equal to the estimated overburden stresses at these points, indicating that excess pore water pressure ratios, r_u, of, or near, 100% were triggered. Under the embankment, the r_u value reached a maximum value of 88%.

The EPWPs began dissipating after the end of the strong shaking period of the motion (time ~25 s) with the dissipation being faster underneath the embankment and between the soil-cement columns than the free field. The faster rate of dissipation in the soil between the soil-cement columns could be due to 1) preferential seepage paths which may have formed along the sides of the columns, or 2) stiffness contrast between the soil and soil-cement columns, which can accelerate pore pressure dissipation by transferring vertical loads from the soil to the columns during consolidation. The recorded EPWP in the free field showed the lowest rate of EPWP dissipation due to the flow of pore water during and after shaking toward the toe of the embankment.

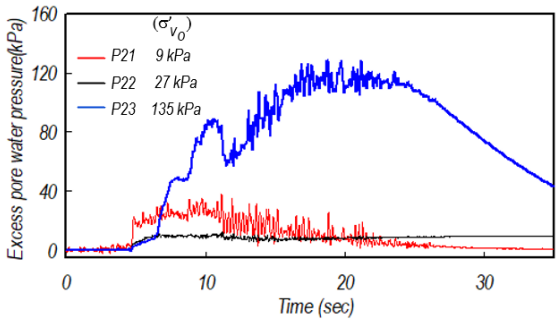

Fig. 6 – Excess pore-water pressures during main shaking PBA=0.4g

3.3 Embankment and Ground Surface Deformation

Cumulative shaking-induced vertical displacements of the embankment crest and free field for all shaking events are presented in Fig. 7. As shown in this figure, the incremental crest settlement of the embankment decreased with the intensity of the shaking event. The incremental shaking-induced settlement of the crest was about 47.6 cm for the motion with PBA=0.40g, while this value for the strongest motion with PBA=0.55g was about 7.4 cm. The settlement of the embankment is attributed to a combination of several contributing mechanisms, including deformation of the liquefied loose sand through the spaces between the soil-cement columns, cracking and tilting of the soil-cement columns, shear deformation of the loose sand layer outside the treatment zone, and post-liquefaction reconsolidation strains in the loose sand layer.

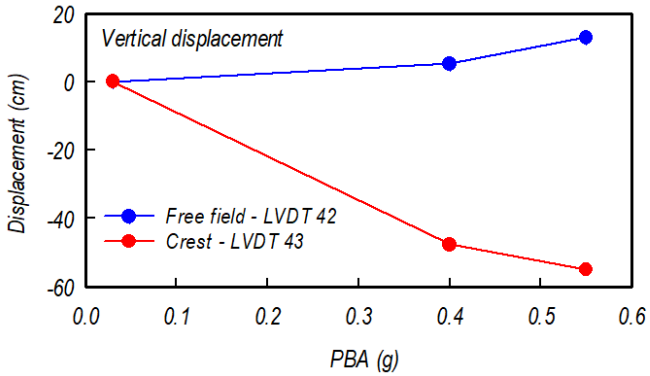

Fig. 7 – Vertical displacement of embankment during different PBA(g)

Fig. 7 also displays the cumulative shaking-induced uplift movement of the soil at the toe of the embankment for all shaking events. The lateral movement of the liquefied soil through the spaces between the soil-cement columns could cause a net lateral compression of the sand between the treatment zone and the container wall. Therefore, the upward movement of the soil foundation in the downstream side of the

embankment could occur. At the toe of the embankment (free field), the shaking-induced uplift was 5.3 cm for motion with PBA = 0.40g and about 13 cm for the strongest motion with PBA=0.55g.

At the end of the test, the embankment was removed from the top of the foundation soil, and the vertical deformation of the soil surface was carefully mapped using a laser surface scanner. Fig. 8 presents vertical displacement at the top of the loose sand layer. These measurements showed large settlements on the embankment side of the foundation and heave (upward movement) of the loose sand on the downstream side of the treatment zone. The settlement of the embankment side was due to the combined influence of shearing deformation toward the toe and post-liquefaction reconsolidation strains in this area.

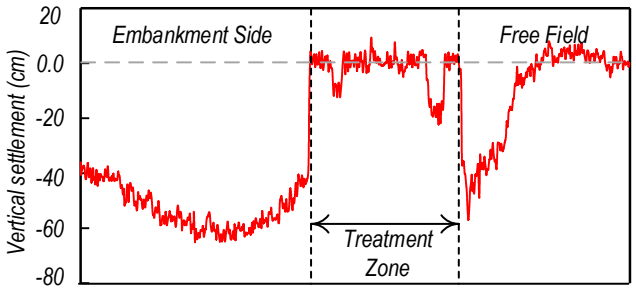

Fig. 3 – Measured vertical displacement on silica sand after the test

3.4 Post-Test Observations

Cracking patterns, location, orientation, number, and distribution of the cracks provided information about the performance of the embankment and soil-cement columns and their possible failure mechanism. Post-test photos of the embankment showed that the majority of embankment cracking formed between the crest and lower 1/3 the slope and propagated across the width of the embankment. The cracking of the embankment is mostly attributed to the post-liquefaction reconsolidation strains in the loose sand layer, as previously discussed in Fig. 8 and lateral deformation of soil-cement columns.

The soil surrounding the soil-cement columns was excavated at the end of the test, and cracking of the columns was mapped to investigate shaking-induced damage to the soil-cement columns and their possible failure modes. An isolated column may fail by shearing, bending, or tilting depending on column location and length, soil-cement material strength, and embankment height. Photographs of the soil-cement columns during model dissection after testing are shown in Fig. 9b. The results of crack detectors and the post-test inspections of soil-cement columns indicated that the majority of damage to the soil-cement columns occurred during the PBA = 0.40g shaking event. As shown in Fig. 9b, dominant failure modes of the soil-cement columns were shear failure and all columns sheared off along their connection with the concrete base layer and tilted toward the toe of the embankment (left side of the figure).

Fig. 9 – (a) Post-test photos of the embankment, and (b) Post-test excavation photos of the soil-cement columns (toe of the embankment is on the left side of photo).

4. Conclusion

Dynamic centrifuge test on an embankment model laid over a saturated loose sand layer and supported by the isolated columns was performed using 3 m radios centrifuge at the National Central University of Taiwan. The model was shaken by three different input motions with different shaking intensities to investigate the seismic performance of the embankment and soil-cement columns.

The recorded acceleration from the embankment crest and foundation soil attenuated compared to input motion due to liquefaction of the loose soil layer. The asymmetric response in the recorded time history at crest was a result of the downslope movement of the embankment. The excess pore water pressure under the embankment reached its maximum value equaled to the overburden pressure and stands far greater than what was measured on the downstream and near the toe of the embankment. The pore water pressure measured in the soil between the columns dissipated faster than what measured under and beyond the embankment. The behavior could be attributed to the stiffness contrast between the soil and soil-cement columns, which can accelerate pore pressure dissipation by transferring vertical loads from the soil to the columns during pore water dissipation. The recorded EPWP in the free field showed the lowest rate of EPWP dissipation due to the flow of pore water during and after shaking toward the toe of the embankment. Post-shaking assessment of the model showed that the majority of the cracks happened at upslope, and in the lower, one-third of the slope where distributed horizontally toward the side of the embankment. These results could be linked to accumulated shear strain in slope triggered by shear and tilting failure of the soil-cement columns.

5. Acknowledgements

The authors appreciate the assistance of the staff of the Centrifuge facility at the National Central University of Taiwan. Any opinions, findings, or recommendations expressed herein are those of the authors and should not be interpreted as representing the official policies, either expressed or implied, of the above organizations. The assistance of the students at the center is also greatly appreciated.

References

[1] Almeida MS, Davies MCR, Parry RHG (1998): Centrifuge tests of embankments on strengthened and unstrengthened clay foundations. *Géotechnique*, Volume 35 Issue 4, December 1985, pp. 425-441

[2] Broms BB (1999): Design of lime, lime/cement, and cement columns. *Keynote lecture In: International conference on dry mix methods: dry mix methods for deep soil stabilization*, Stockholm, Sweden AA, Balkema, Rotterdam, Netherlands, pp 125–153

[3] Kitazume M, Maruyama K (2006): External stability of group column type deep mixing improved ground under embankment loading. *Soils Found* **46** (3):323–340

[4] Kitazume M, Maruyama K (2007): Internal stability of group column type deep mixing improved ground under embankment loading. *Soils Found* **47** (3):437–455

[5] Adalier K., Elgamal AW, Martin GR (1998): Foundation liquefaction countermeasures for earth embankments. *Journal of Geotechnical and Geoenvironmental Engineering*, **124** (6), 500-517.

[6] Khosravi M, Boulanger RW, Wilson DW, Olgun CG, TamuraS, Wang Y (2017): Dynamic centrifuge tests of structures with shallow foundations on soft clay reinforced by soil-cement grids. *Soils and foundations*, **57** (4), 501-513.

[7] Tokimatsu K, Asaka Y (1998): Effects of liquefaction-induced ground displacements on pile performance in the 1995 Hyogoken-Nambu earthquake. *Soils and Foundations*, 38 (Special), 163-177.

[8] Yamashita K, Hamada J, Onimaru S, Higashino M (2012): Seismic behavior of piled raft with ground improvement supporting a base-isolated building on soft ground in Tokyo. *Soils and Foundations*, 52(5), 1000–1015.

[9] Tokunaga S, Kitazume M, Morikawa Y, Takahashi H, Nagatsu T, Honda N, Onishi T, Asanuma T, Kubo S, Higashi S (2015): Performance of cement deep mixing method in 2011 tohoku earthquake. *The Deep Mixing 2015 Conference*, San Francisco, CA, 1071-1080.

[10] Khosravi M, Boulanger RW, Tamura S, Wilson DW, Olgun CG, Wang Y (2016): Dynamic centrifuge tests of soft clay reinforced by soil–cement grids. *Journal of Geotechnical and Geoenvironmental Engineering*, **142** (7), 04016027.

[11] Rayamajhi D, Tamura S, Khosravi M, Boulanger RW, Wilson DW, Ashford SA, Olgun CG (2015): Dynamic centrifuge tests to evaluate reinforcing mechanisms of soil-cement columns in liquefiable sand. *Journal of Geotechnical and Geoenvironmental Engineering*, **141** (6), 04015015.

[12] Mengyi Z, Qiang X, Xinwen C, Wen Z (2019): The Shaking Table Test on the Performance of Cement-mixed Piles in Liquefiable Railway Foundations[J]. *Earthquake Research in China*, **33** (1), 120-131.

[13] Zhou H, Zheng G, Liu J, Yu X, Yang X, Zhang T (2019): Performance of embankments with rigid columns embedded in an inclined underlying stratum. *centrifuge and numerical modelling. Acta Geotechnica*, **14** (5), 1571-1584.

[14] Nguyen B, Takeyama T, Kitazume M (2016): Internal failure of deep mixing columns reinforced by a shallow stabilized soil beneath an embankment. *International Journal of Geosynthetics and Ground Engineering*, **2** (4), 30.

[15] Nguyen B, Takeyama T, Kitazume M (2016): External failure of deep mixing columns reinforced by a shallow layer beneath an embankment. *Journal of JSCE*, **4** (1), 92-105.

[16] Boulanger RW, Khosravi M, Khosravi A, Wilson DW (2018): Remediation of liquefaction effects for an embankment using soil-cement walls. Centrifuge and numerical modeling. *Soil Dynamics and Earthquake Engineering*, 114, 38-50.

[17] Kutter, B. L. (1995): Recent Advances in Centrifuge Modeling of Seismic Shaking (State-of-the-Art Paper), *Proceeding of 3rd International Conference on Recent Advances in Geotechnical Earthquake Engineering and Soil Dynamics*, 2, 927-942.

[18] Tamura S, Khosravi M, Wilson DW, Rayamajhi D, Boulanger RW, Olgun CG, Wang Y (2018): Simple method for detecting cracks in soil-cement reinforcing elements for geotechnical centrifuge tests. *Int J Phys Model Geotech*. **18** (6), 281-289. https://doi.org/10.1680/jphmg.17.00036.

